Available online at www.sciencedirect.com
SCIENCE DIRECT®
Journal of Solid State Chemistry 174 (2003) 264–275
JOURNAL OF SOLID STATE CHEMISTRY
http://elsevier.com/locate/jssc

Solvothermal syntheses, crystal structures, and thermal stability of two new thioantimonates(III) using complex transition metal cations as structure directing agents: the layered compound $[Ni(dien)_2]Sb_4S_7 \cdot H_2O$ and the three-dimensional compound $[Ni(dien)_2]_3Sb_{12}S_{21} \cdot H_2O$

Ralph Stähler, Christian Näther, and Wolfgang Bensch*

Institut für Anorganische Chemie der Christian-Albrechts-Universität Kiel, Olshausenstr. 40, D-24098 Kiel, Germany

Received 15 October 2002; received in revised form 27 December 2002; accepted 14 April 2003

Abstract

The two new thioantimonates(III) $[Ni(dien)_2]Sb_4S_7 \cdot H_2O$ (**I**) and $[Ni(dien)_2]_3Sb_{12}S_{21} \cdot H_2O$ (**II**) were prepared under solvothermal conditions using elemental Ni, Sb, S and an aqueous solution of diethylenetriamine (dien) as solvent. Compound **I** crystallizes in the monoclinic space group $P2_1/c$, $a = 9.603(2)$ Å, $b = 16.137(3)$ Å, $c = 17.272(4)$ Å, $\beta = 91.68(3)^\circ$, $V = 2675.3(9)$ Å^3, $Z = 4$ and compound **II** crystallizes in the monoclinic space group $C2/c$ with $a = 12.6072(7)$ Å, $b = 14.9967(7)$ Å, $c = 41.445(2)$ Å, $\beta = 95.371(6)^\circ$, $V = 7801.4(7)$ Å^3, $Z = 4$. The two-dimensional $^2_\infty[Sb_4S_7^{2-}]$ anion in **I** is composed of two SbS_3 trigonal pyramids and two SbS_4 units. The SbS_3 units are connected via one corner to form a Sb_2S_5 unit and the two SbS_4 moieties share a common edge building a *trans*-Sb_2S_6 unit. The Sb_2S_5 and *trans*-Sb_2S_6 units have one common S atom to form the layered $^2_\infty[Sb_4S_7^{2-}]$ anion. Within the layers Sb_2S_2, Sb_4S_4 and Sb_8S_8 heterorings are found with the *mer*-$[Ni(dien)_2]^{2+}$ residing above and below the large pores. In compound **II** the $^3_\infty[Sb_{12}S_{21}^{6-}]$ anion is composed of four SbS_3 pyramids and two SbS_4 units. The condensation of the different primary units yields Sb_xS_x rings with $x = 2, 3, 4, 8$, and 32. The largest ring consists of 64 atoms ($Sb_{32}S_{32}$) and the pores with an ellipsoidal shape are oriented parallel to the [110] direction. To the best of our knowledge this is the largest Sb_xS_x heteroring found in thioantimonates(III) so far. The cations are located above and below the large ring or within the plane of the ring. Nearly rectangular channels are running along [101] which have dimensions of about $7.6 \cdot 13.5$ Å. The channels are occupied by the water molecule and by the ligands pointing into the channels. The thermal behavior of the compounds was investigated using differential thermoanalysis (DTA), thermogravimetry (TG) and mass spectroscopy (MS) measurements. Upon heating decomposition of the compounds starts at $T_{onset} = 235$°C (I) and $T_{onset} = 258$°C (II). The degradation of the samples proceeds in several steps and the ligands and water molecules are successively emitted. In the X-ray powder patterns of the decomposition products NiS, NiSbS, and Sb_2S_3 could be identified.

Keywords: Thioantimonates; Solvothermal synthesis; Crystal structure; Thermoanalytical measurements

1. Introduction

Despite the structural diversity of thioantimonates (III) the three-dimensional interconnection of the $[Sb_xS_y^{z-}]$ units is rare and mainly restricted to compounds with small cations as charge balancing ions. A good relationship between dimensionality of the thioantimonate(III) anions and the size and charge balancing counterion is observed when alkali or earth alkaline cations are used. Nice examples are the compounds with the $[Sb_4S_7^{2-}]$ anion, i.e., $K_2Sb_4S_7$ [1], $K_2Sb_4S_7 \cdot H_2O$ [2], $Rb_2Sb_4S_7$ [3], $Rb_2Sb_4S_7 \cdot H_2O$ [4], $Cs_2Sb_4S_7$ [5], $SrSb_4S_7 \cdot 6H_2O$ [6], $[NH_4]_2Sb_4S_7$ [7], $[C_4H_8N_2]Sb_4S_7$ [8], $[C_2H_5NH_3]_2Sb_4S_7$ [9] and $[M(C_2H_8N_2)_3]Sb_4S_7$ (M = Mn, Fe, Ni) [10,11]. In $K_2Sb_4S_7$ a three-dimensional network is formed. In the water containing compound, $K_2Sb_4S_7 \cdot H_2O$, a layered $^2_\infty[Sb_4S_7^{2-}]$ anion is observed

*Corresponding author. Fax: +49(0)-431/8801520.
E-mail address: wbensch@ac.uni-kiel.de (W. Bensch).

0022-4596/03/$ - see front matter © 2003 Elsevier Inc. All rights reserved.
doi:10.1016/S0022-4596(03)00216-0

with hydrated K^+ located between the layers. With the larger Rb^+ cation the $^2_\infty[Sb_4S_7^{2-}]$ anion is also layered. The water containing compound $Rb_2Sb_4S_7 \cdot H_2O$ exhibits also a layered thioantimonate(III) anion, but within the $^2_\infty[Sb_4S_7^{2-}]$ layers interconnection of the SbS units is quite different. With larger complex cations as in $[M(C_2H_8N_2)_3]Sb_4S_7$ (M = Mn, Fe, Ni) the anionic part of the structure consists of semicubes linked by a single SbS_3 pyramid into "zig-zag" chains running parallel to the c-axis.

An obvious relation between the dimensionality of the anionic thioantimonate(III) networks and size/charge of organic ions as charge balancing counterions is not observed. This may be due to several factors determining the dimensionality of the anionic part of the structures. Depending on the synthesis conditions the organic molecules may be present as hydrated or solvated aggregates and the true size of these structure directing molecules is significantly larger than estimated from static geometrical parameters.

The dimensionality of the thioantimonate(III) network could often not unambiguously be answered because Sb–S interatomic separations spread from about 2.3 Å up to the sum of the van der Waals radii of about ≈3.8 Å. An analysis of a few dozen thioantimonate(III) compounds reveals that there is no clear cut-off above the Sb–S single bond distance of about 2.5 Å. Several authors tackled the question of the chemical meaning of the long Sb–S separations applying the concept of bond length bond strength relations. For Sb–S distances up to 3.8 Å valence units of about 0.1 are calculated indicating very weak bonding interactions [12].

The three dimensional interconnection of SbS_x moieties is difficult to achieve due to the low flexibility of the angle Sb–S–Sb that ranges from about 80° to 115° and due to the small energetic differences between several thioantimonate(III) compounds. In contrast for oxidic compounds containing TO_4 units (T = Si, Al, Ga etc.) T–O–T angles vary over the very large range from 90° to 180° [13] and it could be easily envisaged that the arrangement around a specific structure directing molecule is much easier achieved.

During the last few years several new and exciting thioantimonates(III) were prepared under solvothermal conditions using organic molecules, but to the best of our knowledge only few attempts were made using complex transition metal cations as structure directing agents. Here we report on the syntheses and crystal structures of the two new thioantimonate(III) compounds $[Ni(dien)_2]Sb_4S_7 \cdot H_2O$ (layered) and the three-dimensional $[Ni(dien)_2]_3Sb_{12}S_{21} \cdot H_2O$ using the in-situ formation of a complex cation as structure directing molecule. We present also results of the investigations of the thermal stability and of Raman spectroscopy.

2. Experimental

2.1. Synthesis

$[Ni(dien)_2]Sb_4S_7 \cdot H_2O$ (dien = diethylenetriamine) **I** was obtained in nearly 40% yield by the reaction of elemental Ni (0.0587 g, 1 mmol), Sb (0.1217 g, 1 mmol) and sulfur (0.096 g, 3 mmol) in an aqueous solution of 2 mL dien (50%) (Merck Chemical). The mixture was heated in Teflon-lined steel autoclaves with an inner volume of 30 mL for 5 days at 140°C and then cooled to room temperature within 3 h. After washing with water and acetone, dried under vacuum, yellow crystals of $[Ni(dien)_2]Sb_4S_7 \cdot H_2O$ were obtained. The product contained as the second phase $[Ni(dien)_2]_3(SbS_4)_2$ (by-product) [14]. Stirring the solution during the syntheses a phase pure product was obtained within 3 h applying Ni:Sb:S in a 0.25:0.25:0.75 mmol (0.0147; 0.0304; 0.0240 g) ratio in an aqueous solution of 2 mL dien (50%) solution at 140°C. The compound is stable on air, in water and in acetone. C, H, N analysis: found: C: 9.38%, H: 2.65%, N: 7.83%; calcd.: C: 9.66%, H: 2.84%, N: 8.45%.

$[Ni(dien)_2]_3Sb_{12}S_{21} \cdot H_2O$ (dien = diethylenetriamine) **II** was first prepared by reacting elemental Ni, Sb and S in 10 mL of an aqueous solution of dien (50%) applying 1 mmol Ni (0.0587 g), 1 mmol Sb (0.1217 g) and 2 mmol S (0.0641 g). The mixture was heated in a Teflon-lined autoclave at 140°C for 7 days. The reaction mixture was filtered off, washed with water and acetone and cleaned in an ultrasonic bath. The yellow crystals were obtained in a 40% yield. The second compound was identified as $[Ni(dien)_2]_3(SbS_4)_2$ [14]. Stirring a mixture of 5 mL 50% dien, 1 mmol Ni, 1 mmol Sb, and 3 mmol S at 120°C for 1 day a microcrystalline powder of $[Ni(dien)_2]_3Sb_{12}S_{21} \cdot H_2O$ is obtained. According to the X-ray powder pattern the product was phase pure. The complex *mer*-$[Ni(dien)_2]Cl_2 \cdot H_2O$ [15] was also used as a precursor to synthesize $[Ni(dien)_2]_3Sb_{12}S_{21} \cdot H_2O$. A typical run consisted of 1 mmol *mer*-$[Ni(dien)_2]Cl_2 \cdot H_2O$ (0.3539 g), Sb (0.1217 g, 1 mmol), and S (0.096 g, 3 mmol) in 10 mL of 50% dien solution. Such mixtures were heated at 140°C for 5 days, then cooled to room temperature, filtered off, washed with water and acetone and yellow crystals were obtained. C, H, N analysis: found: C: 9.00%, H: 2.71%, N: 7.83%; calcd.: C: 9.79%, H: 2.64%, N: 8.56%.

2.2. Crystal structure determination

Intensities were collected on a STOE Imaging Plate Diffraction System (IPDS) using monochromated Mo$K\alpha$ radiation ($\lambda = 0.71073$ Å). The intensities were corrected for Lorentz, polarization and absorption effects. Structure solution was performed using SHELXS-97 [16]. Refinement was done against F^2 using

Table 1
Technical details of data acquisition and selected refinement results for $[Ni(dien)_2]Sb_4S_7 \cdot H_2O$ and $[Ni(dien)_2]_3Sb_{12}S_{21} \cdot H_2O$

Formula	$[Ni(dien)_2]Sb_4S_7 \cdot H_2O$	$[Ni(dien)_2]_3Sb_{12}S_{21} \cdot H_2O$
Color, habit	Yellow polyeder	Yellow polyeder
Molecular weight ($g\,mol^{-1}$)	992.48	2945.43
Crystal system	Monoclinic	Monoclinic
Space group	$P2_1/c$	$C2/c$
Calculated density ($g\,cm^{-3}$)	2.464	2.508
a (Å)	9.603(2)	12.6072(7)
b (Å)	16.137(3)	14.9967(7)
c (Å)	17.272(4)	41.445(2)
β (°)	91.68(3)	95.371(6)
V ($Å^3$)	2675.3(9)	7801.4(7)
Z	4	4
T (K)	293	293
Scan range	$3° \leqslant 2\theta \leqslant 56°$	$4° \leqslant 2\theta \leqslant 52°$
	$0 \leqslant h \leqslant 12$	$-15 \leqslant h \leqslant 15$
	$-21 \leqslant k \leqslant 1$	$-18 \leqslant k \leqslant 18$
	$-22 \leqslant l \leqslant 22$	$-50 \leqslant l \leqslant 50$
Measured reflections	7559	29,577
Independent reflections	6466	7562
Reflections with $F_o > 4\sigma(F_o)$	5352	6705
μ (mm^{-1})	5.238	5.385
$R_{int.}$	0.0399	0.0932
Min./max. trans.	0.4018, 0.5600	0.4465, 0.5471
Weight[a]	$y = 0.0389$, $z = 3.2408$	$y = 0.0374$, $z = 10.2883$
R_1 for all $F_o > 4\sigma(F_o)$	0.0286	0.0295
R_1 for all reflections	0.0420	0.0345
wR_2 for all $F_o > 4\sigma(F_o)$	0.0701	0.0702
wR_2 all reflections	0.0738	0.0728
Residual electron density ($e/Å^3$)	−0.82/0.90	−1.06/1.09
Goodness of fit	1.059	1.030

[a] $w = 1/[\sigma^2(F_o^2) + (y \cdot P)^2 + z \cdot P]$; $P = (Max(F_o^2, 0) + 2F_c^2)/3$.

SHELXL-97 [17]. Absorption corrections were performed using X-SHAPE [18]. All heavy atoms were refined anisotropically. The hydrogen atoms were positioned with idealized geometry and refined with fixed isotropic displacement parameters using a riding model. The hydrogen atoms were positioned at 0.91 Å (secondary amino groups) or at 0.90 Å (primary amino groups) (Table 4). Technical details of data acquisition and refinement results are summarized in Table 1.

2.3. Thermoanalytical measurements

Thermoanalytical measurements were performed using a DTA-TG device STA 429 from Netzsch. All measurements were performed in an argon atmosphere (flow rate 50 mL min^{-1}) with Al_2O_3 crucibles and heating rates of 3 K min^{-1}.

DTA-TG-MS measurements were performed simultaneously using the STA-409CD with Skimmer coupling from Netzsch, which is equipped with a quadrupole mass spectrometer QMA 400 (max. 512 amu) from Balzers. The MS measurements were performed in analog and trend scan mode. All measurements were corrected for buoyancy and current effects and were performed using heating rates of 4 K min^{-1}. In Al_2O_3 crucibles under a dynamic helium atmosphere (flow-rate: 75 mL min^{-1}, purity: 4.6).

2.4. Raman spectra

Raman spectra were measured in the region from 100 to 3500 cm^{-1} with a Bruker IFS 66 Fourier transform Raman spectrometer.

2.5. X-ray powder diffractometry

The X-ray powder patterns were recorded on a STOE Stadi-P diffractometer (Cu$K\alpha_1$ radiation, $\lambda = 1.540598$ Å) in transmission geometry.

Crystallographic data (excluding structure factors) for the structure reported in this paper have been deposited with the Cambridge Crystallographic Data Center as supplementary publication no. CCDC 188434 for **I** and no. CCDC 188433 for **II**. Copies of the data can be obtained free of charge on application to CCDC, 12 Union Road, Cambridge CB2 1 EZ, UK [Fax: +44-(0)1223-336033 or email: deposit@ccdc.cam.ac.uk].

3. Results and discussion

3.1. Syntheses

The solvothermal syntheses were first performed applying the educts in elemental form. In further experiments the complex *mer*-$[Ni(dien)_2]Cl_2 \cdot H_2O$ [15] was introduced instead of elemental Ni. Interestingly, the title compounds could also be prepared using this transition metal complex. One important conclusion of the investigations is that the redox reaction between Ni and the polysulfides formed in the very basic solutions seems to play no role for the product formation. Whereas in compound **I** the complex still shows the *mer*-configuration an isomerization to the *u-fac* and *s-fac* configurations is observed in compound **II**. The heterogeneous reactions occurring under solvothermal conditions are complex and for the present compounds there is no simple explanation at hand how the experimental factors influence and determine the product formation. About 100 syntheses were performed

where the amount and concentration of the amine were varied and the Ni:Sb:S ratio as well as the temperature were held constant. The results of the experiments gave hints that crystallization of compound **II** is favored applying larger amounts of the amine. In-situ X-ray scattering experiments are planned to investigate the formation of the two compounds more in detail.

3.2. Crystal structures

For many thioantimonates(III) the structures are constructed by successive condensation of primary and secondary building units. Hence, the description of the crystal structures of thioantimonate(III) networks is best performed starting with the interconnection of the primary building units SbS_x ($x = 3-6$) (PBU) that form secondary building blocks (SBU). These SBU's are often Sb_xS_x heterorings or the so-called Sb_3S_4 semicubes.

For the presentation of the structures of the title compounds all Sb–S distances longer than about 3 Å are neglected in the first approach.

In compound **I** the octahedral $[Ni(dien)_2]^{2+}$ cation (dien = diethylenetriamine) adopts the *mer*-configuration (Fig. 1a). In **II** there are two crystallographically independent $[Ni(dien)_2]^{2+}$ cations with one cation (Ni(1)) in the *u-fac* configuration (Fig. 1b) and the second cation (Ni(2)) adopting the *s-fac* configuration (Fig. 1c). The Ni–N distances in **I** vary between 2.076(4) and 2.170(4) Å (Table 2) with N–Ni–N angles ranging from 80.1(2)° and 99.9(2)°.

In **II** the Ni–N distances are between 2.097(3) and 2.150(4) Å (Table 2) with N–Ni–N angles between 80.2(2)° and 98.3(2)°. Angles and distances are comparable with those reported in Refs. [14,19]. We note that dien complexes of transition metal ions have been known for a long time [20,21] and the geometric isomers of the cations were intensively studied [22–27].

The $^2_\infty[Sb_4S_7^{2-}]$ anion in compound **I** is composed of two SbS_3 trigonal pyramids and two SbS_4 units. The two SbS_3 (Sb(1) and Sb(2)) units share a common corner to form a Sb_2S_5 unit (Fig. 2). The Sb–S bond lengths range from 2.385(1) to 2.477(1) Å, and the S–Sb–S angles vary between 91.00(4)° and 104.52(4)° (Table 2) [28,29]. The two SbS_4 units (Sb(3) and Sb(4)) are joined by a common edge forming a *trans*-Sb_2S_6 moiety with a central Sb_2S_2 heteroring (Fig. 2). In the SbS_4 units both Sb atoms have two short (2.387(1) and 2.440(1) Å for Sb(3), 2.386(1) and 2.447(1) Å for Sb(4)) and two significantly longer Sb–S separations of 2.689(1) and 2.815(1) for Sb(3) and 2.721(1) and 2.743(1) Å for Sb(4) (Table 2). The longer Sb–S distances are in *trans*-position with angles S(5)–Sb(3)–S(7) of 172.21(4)° and S(1b)–Sb(4)–S(6) of 174.33(3)° (Table 2). We note that SbS_4 units are not uncommon and Sb–S distances between 2.4 and 2.85 Å were reported, e.g., for

Table 2
Selected distances (Å) and angles (°) for $[Ni(dien)_2]Sb_4S_7 \cdot H_2O$

Sb(1)–S(1)	2.401(1)	Sb(1)–S(2)	2.443(1)
Sb(1)–S(3)	2.477(1)	Sb(2)–S(3)	2.468(1)
Sb(2)–S(4)	2.457(1)	Sb(2)–S(5)	2.385(1)
Sb(3)–S(2a)	2.440(1)	Sb(3)–S(5)	2.815(1)
Sb(3)–S(6)	2.387(1)	Sb(3)–S(7)	2.689(1)
Sb(4)–S(1b)	2.743(1)	Sb(4)–S(4c)	2.447(1)
Sb(4)–S(6)	2.721(1)	Sb(4)–S(7)	2.386(1)
Ni–N(1)	2.092(4)	Ni–N(2)	2.170(4)
Ni–N(3)	2.131(4)	Ni–N(4)	2.076(4)
Ni–N(5)	2.129(4)	Ni–N(6)	2.158(4)
S(1)–Sb(1)–S(2)	99.75(5)	S(1)–Sb(1)–S(3)	92.65(4)
S(2)–Sb(1)–S(3)	92.22(4)	S(3)–Sb(2)–S(4)	91.00(4)
S(3)–Sb(2)–S(5)	92.59(4)	S(4)–Sb(2)–S(5)	104.52(4)
S(2a)–Sb(3)–S(5)	89.84(4)	S(2a)–Sb(3)–S(6)	101.30(4)
S(2a)–Sb(3)–S(7)	85.01(4)	S(5)–Sb(3)–S(6)	88.15(4)
S(5)–Sb(3)–S(7)	172.21(4)	S(6)–Sb(3)–S(7)	87.14(4)
S(1b)–Sb(4)–S(4c)	89.83(3)	S(1b)–Sb(4)–S(6)	174.33(3)
S(1b)–Sb(4)–S(7)	91.57(4)	S(4c)–Sb(4)–S(6)	85.45(4)
S(4c)–Sb(4)–S(7)	102.68(4)	S(6)–Sb(4)–S(7)	86.42(4)
Additional long Sb–S bonds (Å)			
Sb(1)–S(5a)	3.148(1)	Sb(2)–S(1a)	3.283(1)

Symmetry codes: a: $-x, -0.5+y, 1.5-z$, b: $1-x, -0.5+y, 1.5-z$, c: $1+x, y, z$.

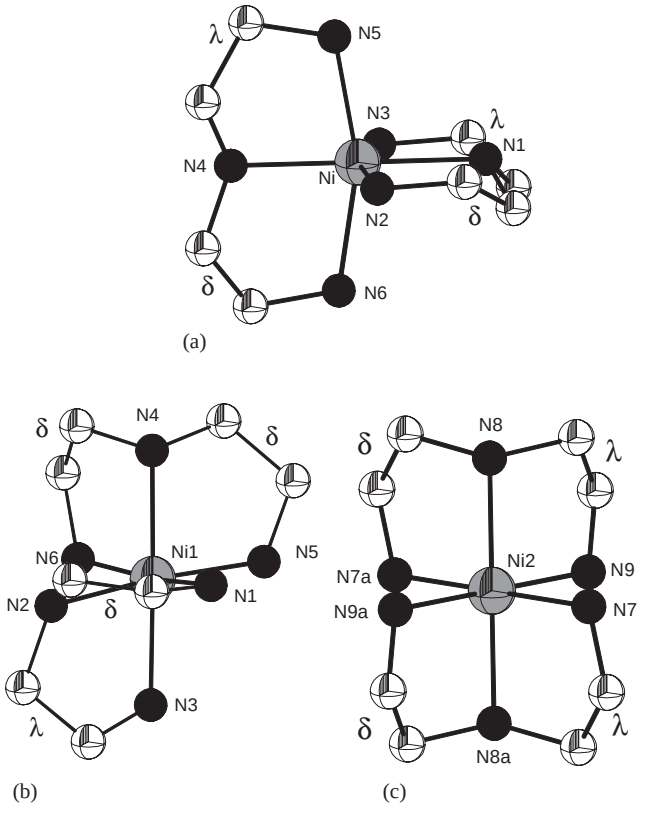

Fig. 1. (a) *mer*-$[Ni(dien)_2]^{2+}$ of $[Ni(dien)_2]Sb_4S_7$ H_2O (**I**), (b) *u-fac*-$[Ni(dien)_2]^{2+}$ and (c) *s-fac*-$[Ni(dien)_2]^{2+}$ of $[Ni(dien)_2]_3Sb_{12}S_{21} \cdot H_2O$ (**II**). Symmetry code: a $(-x, 1-y, 1-z)$ (hydrogen atoms are omitted for clarity).

$(CH_3NH_3)_2Sb_8S_{13}$ [30], $Cs_5Sb_8S_{18}(HCO_3)$ [31], $[Co(C_6H_{18}N_4)]_2Sb_4S_8$ [32] and $[Fe(C_4H_{13}N_3)_2]$ $Sb_6S_{10}\cdot 0.5H_2O$ [33].

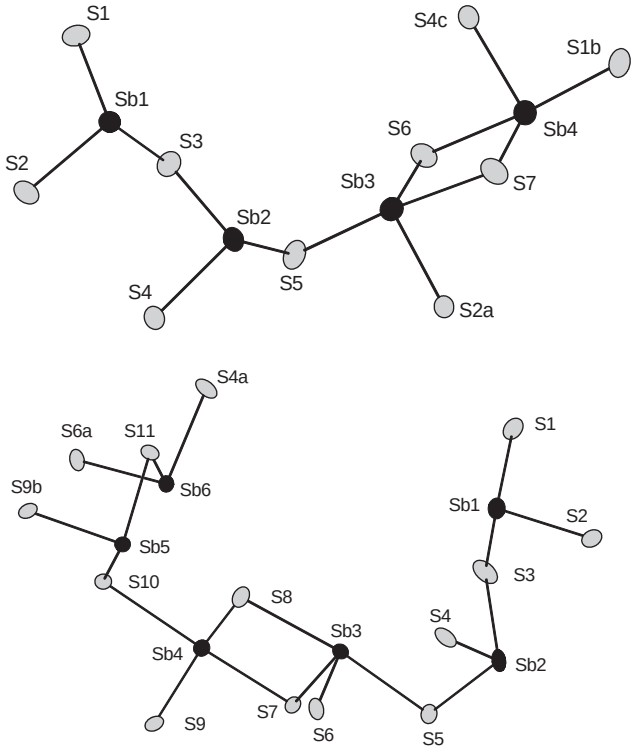

Fig. 2. Top: the primary building units SbS_3 and SbS_4 and their condensation in $[Ni(dien)_2]Sb_4S_7\cdot H_2O$ (**I**) together with labelling. The symmetry codes are given in Table 2. Bottom: the different SbS_x primary building units in $[Ni(dien)_2]_3Sb_{12}S_{21}\cdot H_2O$ (**II**) with numbering scheme. The symmetry codes are given in Table 3. Displacement ellipsoids are drawn at the 50% probability level.

The Sb_2S_5 and Sb_2S_6 share the S(5) atom (Fig. 2) and further interconnection yields the central nearly ellipsoidal shaped Sb_8S_8 ring (Fig. 3). The Sb_8S_8 rings are condensed to each other parallel to the *a*- and *b*-axis to form the layered $^2_\infty[Sb_4S_7^{2-}]$ anion. The condensation generates additional eight-membered Sb_4S_4 rings (see Fig. 3). The thioantimonate(III) layers may be also viewed as a net composed of condensed Sb_2S_2, Sb_4S_4, and Sb_8S_8 heterorings.

Four Sb_4S_4 rings are located at the corners of the nets. Parallel to the *a*-axis neighbored Sb_4S_4 rings are connected via Sb_2S_2 rings and parallel to the *b*-axis they are joined by the S(3) atom parallel to the *b*-axis, thus producing the large Sb_8S_8 rings having pores with a diameter of about $9.60\cdot 7.61$ Å (measured from coordinate to coordinate) (Fig. 3). The layers are stacked perpendicular to the *c*-axis to form channels running along [001]. The shortest interlayer separation is 4.9 Å. The *mer*-$[Ni(dien)_2]^{2+}$ cations and the water molecule are located above and below the large Sb_8S_8 rings thus leading to a sandwich-like arrangement of the thioantimonate anion and the cations. Analyzing the orientation of the cation and the shape and size of the Sb_8S_8 ring the structure directing effect of the cation becomes obvious (Fig. 3). Due to the arrangement of cations and anions H···S contacts between 2.511 and 2.983 Å and angles N–H···S ranging from 130.14° to 171.69° are found that are indicative for weak hydrogen bonding (Table 4).

The Sb(1) and Sb(2) atoms in **I** enhance their coordination numbers from three to four with Sb–S distances ranging from 3.148(1) to 3.283(1) Å (Table 2) to form ψ-SbS_4 trigonal bipyramids (Fig. 6a and b) (sum of the van der Waals' radii of Sb_{vdw} and $S_{vdw} \approx 3.85$ Å

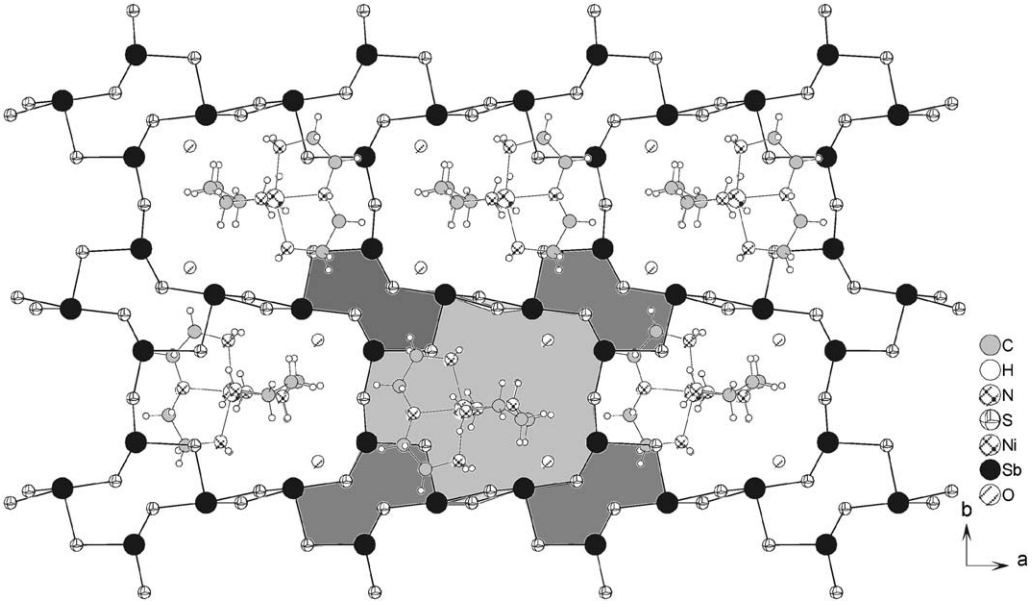

Fig. 3. The crystal structure of $[Ni(dien)_2]Sb_4S_7\cdot H_2O$ (**I**) viewed along [001] with the Sb_2S_2, Sb_4S_4 and Sb_8S_8 heterorings (shaded areas). The cations are located above and below the Sb_8S_8 rings.

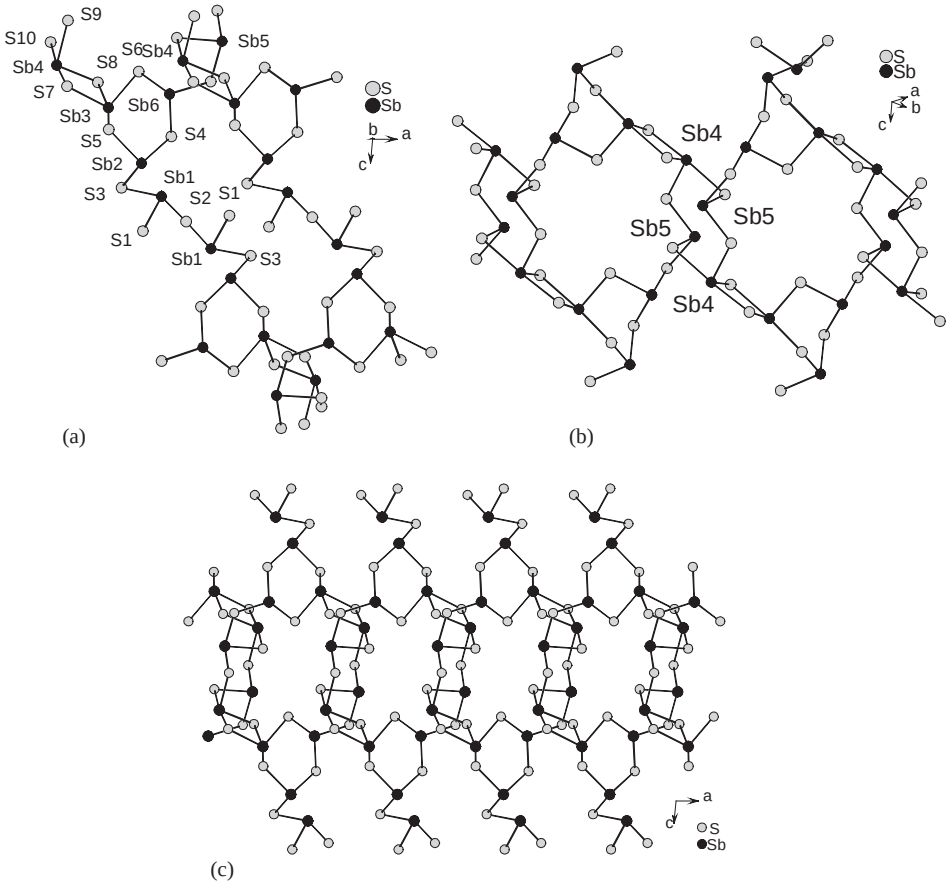

Fig. 4. (a) Interconnection of SbS_3 and SbS_4 units in $[Ni(dien)_2]_3Sb_{12}S_{21} \cdot H_2O$ (**II**) showing the puckered Sb_3S_3 ring and the interconnection of these rings via the Sb_2S_5 unit. (b) The Sb_2S_2, Sb_3S_3, Sb_4S_4 and Sb_8S_8 heterorings in $[Ni(dien)_2]_3Sb_{12}S_{21} \cdot H_2O$ (**II**). (c) The condensation of the different primary units within the (010) plane.

[34]). It is noted that the presence of short and long Sb–S distances is often observed in antimony sulfides and the longer Sb–S separations links building blocks yielding higher structural units.

Several thioantimonates(III) with the $[Sb_4S_7^{2-}]$ anion were reported in the past. As a short summary the dimensionalities of the anion range from three-dimensional networks to one-dimensional chains (Table 5), depending on the size and charge of the balancing cations. For $K_2Sb_4S_7$ (1) a three-dimensional interconnection of one SbS_3 and one SbS_4 unit is observed and Sb_2S_2, Sb_6S_6 and $Sb_{14}S_{14}$ heterorings are found. In $K_2Sb_4S_7 \cdot H_2O$ [2] layers consisting of one SbS_3, three SbS_4 as PBU and Sb_2S_2, Sb_3S_3, Sb_6S_6 and $Sb_{10}S_{10}$ heterorings as SBU's are observed. The layered $Rb_2Sb_4S_7$ [3] compound is constructed of two SbS_4 moieties yielding Sb_2S_2 and Sb_8S_8 rings. In $Rb_2Sb_4S_7 \cdot H_2O$ [4] the anionic layer is constructed by two SbS_3 and two SbS_4 units that are condensed to form Sb_2S_2, Sb_3S_3, Sb_6S_6, and $Sb_{12}S_{12}$ heterorings. The anionic chain in $Cs_2Sb_4S_7$ [5] is composed of two SbS_3 and two SbS_4 units and only a Sb_2S_2 heteroring is observed. A double layer anion is found in $SrSb_4S_7 \cdot 6H_2O$ [6] consisting of three SbS_3 and one SbS_4 unit with Sb_2S_2, Sb_3S_3, and Sb_8S_8 rings as SBU's. In all $[L]Sb_4S_7$ compounds with $L = NH_4^+$, $L = [C_4H_8N_2]$ and $L = [M(C_2H_8N_2)_3]^{2+}$ ($M = Mn, Fe, Ni$) [7,8,10,11] chains are formed which are composed of SbS_3 units and Sb_3S_3 heterorings. Only for $L = EA$ a two-dimensional interconnection was observed [9]. In compound **I** three SbS_3 pyramids and one SbS_4 moiety are connected into Sb_2S_2, Sb_4S_4, and Sb_8S_8 heterorings as SBU'S. In summary: None of the 12 compounds contain an isolated $[Sb_4S_7^{2-}]$ anion and only one three-dimensional $^3_\infty[Sb_4S_7^{2-}]$ anion was found with the small K^+ ion. In all layered anions Sb_xS_x rings with x between 2 and 14 are observed. In chain-like anions Sb_3S_3 heterorings are found with the exception of $Cs_2Sb_4S_7$ which contains only a Sb_2S_2 ring.

In **II** the 6 unique Sb(III) atoms have bonds to either three (Sb(1), Sb(2), Sb(5), Sb(6)) or to four S atoms (Sb(3), Sb(4)) forming SbS_3 trigonal pyramids and SbS_4 moieties (see Figs. 2 and 4). The Sb–S distances within the SbS_3 pyramids are between 2.339(2) and 2.541(1) Å with S–Sb–S angles ranging from 85.84(4)° to 101.67(4)° (Table 3). For the two SbS_4 units the Sb–S bond lengths scatter over a rather large range with remarkable differences. The Sb(3) atom is surrounded by two S

Table 3
Selected distances (Å) and angles (°) for $[Ni(dien)_2]_3Sb_{12}S_{21} \cdot H_2O$

Sb(1)–S(1)	2.339(2)	Sb(1)–S(2)	2.480(1)
Sb(1)–S(3)	2.482(2)	Sb(2)–S(3)	2.440(2)
Sb(2)–S(4)	2.442(1)	Sb(2)–S(5)	2.376(1)
Sb(3)–S(5)	2.703(1)	Sb(3)–S(6)	2.438(1)
Sb(3)–S(7)	2.4280(9)	Sb(3)–S(8)	2.765(1)
Sb(4)–S(7)	2.612(1)	Sb(4)–S(8)	2.356(1)
Sb(4)–S(9)	2.443(1)	Sb(4)–S(10)	2.913(1)
Sb(5)–S(9b)	2.487(1)	Sb(5)–S(10)	2.394(1)
Sb(5)–S(11)	2.524(1)	Sb(6)–S(4a)	2.541(1)
Sb(6)–S(6a)	2.421(1)	Sb(6)–S(11)	2.429(1)
Ni(1)–N(1)	2.118(4)	Ni(1)–N(2)	2.138(4)
Ni(1)–N(3)	2.105(4)	Ni(1)–N(4)	2.133(3)
Ni(1)–N(5)	2.101(4)	Ni(1)–N(6)	2.148(4)
Ni(2)–N(7)	2.097(3)	Ni(2)–N(8)	2.105(4)
Ni(2)–N(9)	2.150(4)		
S(1)–Sb(1)–S(2)	101.67(4)	S(1)–Sb(1)–S(3)	96.71(5)
S(2)–Sb(1)–S(3)	95.32(4)	S(3)–Sb(2)–S(5)	100.81(4)
S(4)–Sb(2)–S(5)	96.42(4)	S(3)–Sb(2)–S(4)	95.28(5)
S(6)–Sb(3)–S(7)	97.22(4)	S(5)–Sb(3)–S(7)	85.14(3)
S(5)–Sb(3)–S(6)	92.97(4)	S(7)–Sb(3)–S(8)	83.58(3)
S(6)–Sb(3)–S(8)	90.37(4)	S(5)–Sb(3)–S(8)	168.55(3)
S(8)–Sb(4)–S(9)	103.75(6)	S(7)–Sb(4)–S(8)	88.44(3)
S(7)–Sb(4)–S(9)	91.43(4)	S(8)–Sb(4)–S(10)	86.10(3)
S(9)–Sb(4)–S(10)	87.96(3)	S(7)–Sb(4)–S(10)	174.20(3)
S(9b)–Sb(5)–S(10)	97.01(5)	S(9b)–Sb(5)–S(11)	91.82(4)
S(10)–Sb(5)–S(11)	91.95(4)	S(4a)–Sb(6)–S(6a)	93.66(4)
S(4a)–Sb(6)–S(11)	85.84(4)	S(6a)–Sb(6)–S(11)	97.67(4)
Additional long Sb–S bonds (Å)			
Sb(1)–S(1c)	3.751(2)	Sb(1)–S(4)	3.567(1)
Sb(3)–S(4)	3.532(1)	Sb(5)–S(8)	3.246(1)
Sb(5)–S(10d)	3.089(1)	Sb(6)–S(10)	3.029(1)
Sb(6)–S(5a)	3.532(1)		

Symmetry codes: a: $-0.5+x, -0.5+y, z$, b: $1-x, 1-y, 1-z$, c: $2-x, y, 1.5-z$, d: $1-x, 1-y, 1-z$.

atoms at 2.4280(9) and 2.438(1) Å and two S atoms at longer distances of 2.703(1) and 2.765(1) Å with the latter being in *trans* position to each other with S–Sb(3)–S angles scattering between 83.58(3)° to 168.55(3)°. For the Sb(4) atom the environment is more unsymmetrical with short Sb–S bonds of 2.356(1) and 2.443(1) Å, one Sb–S distance of medium length (2.612(1) Å) and a long separation of 2.913(1) Å. Again, the two longer distances are in *trans* position to each other (Table 3).

A central unit of the structure is the puckered Sb_3S_3 heteroring formed by corner sharing of the $Sb(2)S_3$, $Sb(3)S_4$ and $Sb(6)S_3$ units (Fig. 4a). The $Sb(1)S_3$ pyramid is corner-linked to a symmetry related $Sb(1)S_3$ pyramid to form a Sb_2S_5 unit. The two SbS_4 (Sb(3) and Sb(4)) moieties share a common edge yielding a *cis*-Sb_2S_6 unit with a Sb_2S_2 ring. Two Sb_3S_3 rings are linked within the (010) plane by the Sb_2S_5 unit yielding the sequence Sb_3S_3(ring)–Sb_2S_5(chain)–Sb_3S_3(ring) (Fig. 4a). Further interconnection is achieved via a puckered Sb_4S_4 ring composed of two $Sb(4)S_4$ and two $Sb(5)S_3$ building blocks (Fig. 4b) leading to the final arrangement of the different SbS units within the (010) plane in the order Sb_4S_4–Sb_3S_3–Sb_2S_5–Sb_3S_3–Sb_4S_4 (Fig. 4c).

The interconnection into the third direction is achieved via S atoms bound to the Sb atoms of the Sb_4S_4 ring (Sb(4) and Sb(5)). Due the condensation of the different primary units Sb_xS_x rings with $x = 2, 3, 4, 8$, and 32 are formed (Fig. 5, top). The largest ring consists of 64 atoms ($Sb_{32}S_{32}$) and the ellipsoidal pores are parallel to the [110] direction (Fig. 5, top). To the best of our knowledge this is the largest Sb_xS_x heteroring found in thioantimonates(III) so far. The cations are located above and below the large ring (Ni(1)) or within the plane of the ring (Ni(2)). A view along [101] reveals that nearly rectangular channels are formed with dimensions of approximately $7.6 \cdot 13.5$ Å (Fig. 5, bottom). The channels are occupied by the water molecule and by the ligands pointing into the channels. The H···S separations ranging from 2.331 to 2.933 Å with N–H···S angles between 126.5° and 168.51° indicate weak hydrogen bonding (Table 4).

The structure of $[Ni(dien)_2]_3Sb_{12}S_{21} \cdot H_2O$ **II** becomes more complex when the secondary Sb–S bonds are considered. The Sb(1), Sb(5), and Sb(6) atoms have two additional S atoms at distances between 3.029(1) and 3.751(2) Å forming ψ-octahedra (Fig. 6c, e, f, Table 3), and the Sb(3) atom has one long bond to a S atom at a distance of 3.532(1) Å to give also a ψ-octahedral environment (Fig. 6d, Table 3). Note that up to 3.8 Å no such contacts are observed for Sb(2) and Sb(4) (Table 5).

3.3. Thermal investigations

The thermal properties of both compounds were investigated using simultaneous DTA-TG-MS measurements (Fig. 7). Heating $[Ni(dien)_2]Sb_4S_7 \cdot H_2O$ (**I**) a complex thermal behavior is found. Starting at about 90°C a smooth mass decrease is observed in the TG curve which corresponds to the loss of water ($m/z = 18$) and which is finished at about 160°C. The experimental mass loss of about 1.6% (not shown in Fig. 7) is in good agreement with that calculated ($-\Delta m_{theo}$1 $H_2O = 1.8\%$). At about 180°C a strong mass change of about 22.3% is observed in the TG curve which is accompanied by two endothermic events in the DTA curve. From the DTG curve it is obvious that this reaction contains at least two different steps which cannot be successfully resolved. The simultaneous recorded masses demonstrate that in both steps the organic ligand is removed ($m/z = 73$ and 18) and that in the second a small amount of H_2S is released ($m/z = 34$). On further heating a third TG step is observed ($-\Delta m = 3.2\%$) in an endothermic reaction where also small amounts of dien and H_2S are emitted ($m/z = 18$, 34, 73). The total experimental mass loss of about 25.6% is slightly larger than expected if only the

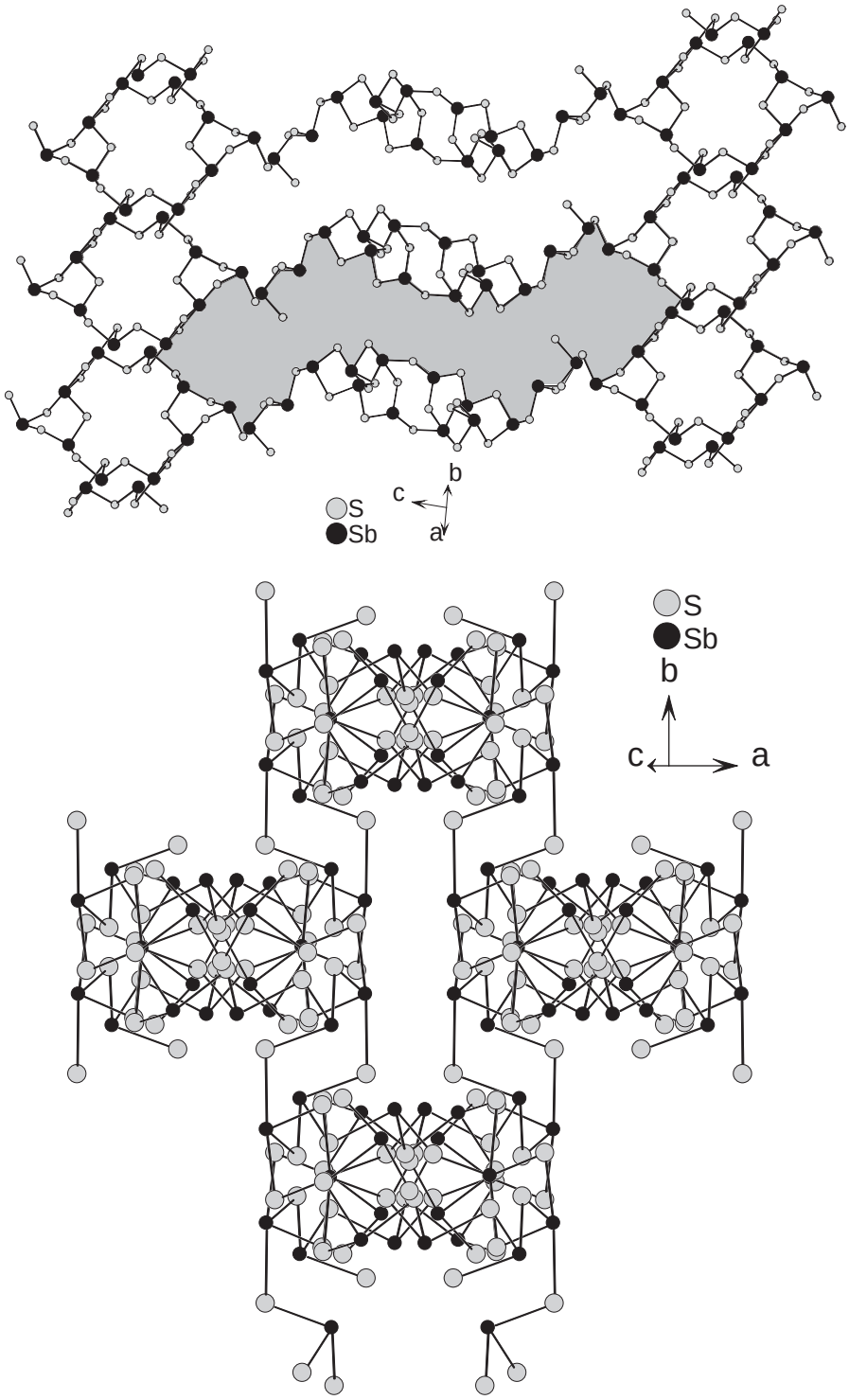

Fig. 5. Top: the large heteroring consisting of 64 atoms ($Sb_{32}S_{32}$, shaded area) in $[Ni(dien)_2]_3Sb_{12}S_{21} \cdot H_2O$ (**II**) with view parallel to [110]. Bottom: the nearly rectangular channels extending in the [101] direction. The cations and the H_2O molecules are omitted for clarity.

organic ligands were removed (($-\Delta m_{theo}$2 dien) = 20.8%). But in agreement with the MS investigations also some sulfur is emitted explaining the differences. According to elemental analysis the final product of these reactions contains practically no C, H and N and X-ray powder diffraction investigations show that the residue is composed of a mixture of NiS, NiSbS and Sb_2S_3.

If the reaction is stopped at 246°C the X-ray powder pattern of the residue is dominated by two very broad and featureless reflections located at about 8° and 17.5° 2θ. In addition, crystalline NiSbS and Sb were identified

Table 4
Proposed hydrogen bonding geometry for $[Ni(dien)_2]Sb_4S_7 \cdot H_2O$ and $[Ni(dien)_2]_3Sb_{12}S_{21} \cdot H_2O$

$D-H$	A	$d(H\cdots A)$	$<DHA$	$d(D\cdots A)$	Symmetry code
$[Ni(dien)_2]Sb_4S_7 \cdot H_2O$					
N2–H2N2	S(2)	2.835	130.14	3.484	$x+1,-y+3/2,z-1/2$
N3–H2N3	S(2)	2.612	171.69	3.505	$x+1,y,z$
N4–H1N4	S(3)	2.635	145.52	3.424	$x+1,y,z$
N2–H1N2	S(4)	2.772	160.99	3.635	$x+1,-y+3/2,z-1/2$
N3–H1N3	S(4)	2.739	135.65	3.441	$x+1,y,z$
N3–H1N3	S(6)	2.838	144.97	3.612	
N6–H1N6	S(6)	2.627	160.16	3.487	
N6–H2N6	S(6)	2.511	168.15	3.397	$-x+1,-y+1,-z+1$
N5–H1N5	S(7)	2.624	149.82	3.432	$x,-y+3/2,z-1/2$
N5–H2N5	S(7)	2.983	167.24	3.866	$-x+1,y+1/2,-z+3/2$
N1–H1N1	O	2.203	158.96	3.070	
$[Ni(dien)_2]_3Sb_{12}S_{21} \cdot H_2O$					
N1–H1N1	S(1)	2.568	155.27	3.406	$-x+3/2,y-1/2,-z+3/2$
N5–H2N5	S(1)	2.628	158.11	3.480	
N5–H1N5	S(2)	2.933	139.90	3.667	$x-1/2,y-1/2,z$
N3–H2N3	S(3)	2.724	146.27	3.508	$-x+3/2,y-1/2,-z+3/2$
N1–H2N1	S(4)	2.576	160.42	3.438	$x-1/2,y-1/2,z$
N6–H2N6	S(5)	2.794	138.31	3.517	$x+1/2,y-1/2,z$
N7–H1N7	S(6)	2.754	126.50	3.368	$x-1/2,y-1/2,z$
N2–H1N2a	S(7)	2.589	161.52	3.464	$x+1/2,y-1/2,z$
N8–H1N8a	S(7)	2.624	159.39	3.491	$x-1/2,y-1/2,z$
N9–H1N9a	S(10)	2.855	168.51	3.741	
N7–H2N7	S(9)	2.558	152.81	3.383	$x-1/2,y-1/2,z$
N9–H2N9a	S(9)	2.668	142.32	3.425	$-x+1/2,-y+3/2,-z+1$
N4–H1N4	S(11)	2.685	160.90	3.558	
N3–H1N3	O	2.331	156.40	3.176	
N6–H1N6	O	2.452	145.75	3.236	

Symmetry code: a: $-x, 1-y, 1-z$.

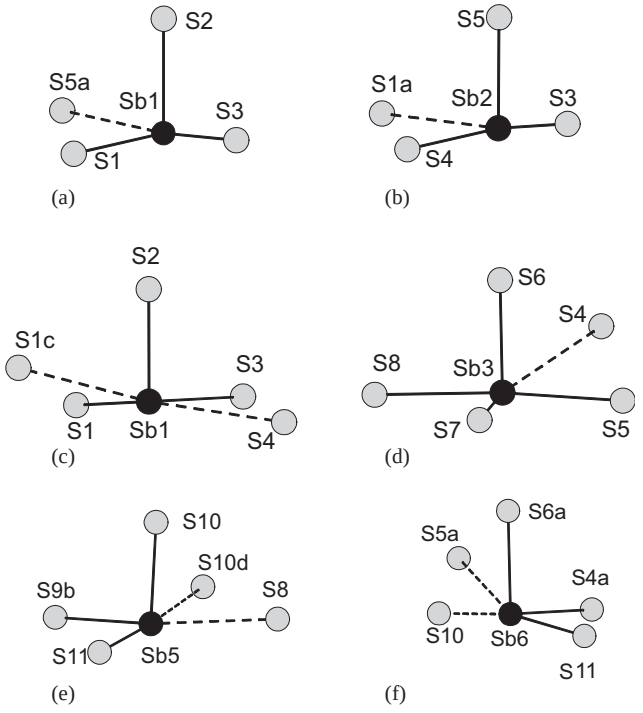

Fig. 6. The environments of the Sb atoms with their long secondary bonds (dotted lines). $[Ni(dien)_2]Sb_4S_7 \cdot H_2O$ (**I**) (a,b), $[Ni(dien)_2]_3Sb_{12}S_{21} \cdot H_2O$ (**II**) (c–f). The symmetry codes are given in Tables 2 and 3.

Table 5
Primary building units (PBU) and secondary building units (SBU) of the $^{x}_{\infty}[Sb_4S_7]$ compounds. References are given in parentheses

	PBU's			SBU's		
	d	SbS_3	SbS_4	Sb_2S_2	Sb_3S_3	Sb_xS_x rings
$K_2Sb_4S_7$ [1]	3	1	1	X	—	Sb_6S_6, $Sb_{14}S_{14}$
$K_2Sb_4S_7 \cdot H_2O$ [2]	2	1	3	X	X	Sb_6S_6, $Sb_{10}S_{10}$
$SrSb_4S_7 \cdot 6H_2O$ [6]	2	3	1	X	X	Sb_8S_8
$Rb_2Sb_4S_7 \cdot H_2O$ [4]	2	2	2	X	X	Sb_6S_6, $Sb_{12}S_{12}$
$[ea]_2Sb_4S_7$ [9]	2	3	1	—	—	Sb_4S_4, Sb_8S_8
$Rb_2Sb_4S_7$ [3]	2	0	2	X	—	Sb_8S_8
$[Ni(dien)_2]Sb_4S_7 \cdot H_2O$	2	2	2	X	—	Sb_4S_4, Sb_8S_8
$Cs_2Sb_4S_7$ [5]	1	2	2	X	—	—
$[NH_4]_2Sb_4S_7$ [7]	1	4	—	—	—	—
$[pip]Sb_4S_7$ [8]	1	3	—	—	X	—
$[Mn(en)_3]Sb_4S_7$ [10]	1	4	—	—	X	—
$[Fe(en)_3]Sb_4S_7$ [11]	1	4	—	—	X	—
$[Ni(en)_3]Sb_4S_7$ [11]	1	4	—	—	X	—

d = dimensionality, ea = ethylamine, pip = piperidine, en = ethylenediamine.

and elemental analysis yields 6.7% C, 1.5% H and 5.2% N. However, no vibrations could be detected in the IR spectrum. If the reaction is quenched at 274°C crystalline NiS, NiS_2, NiSbS and Sb_2S_3 were identified in the

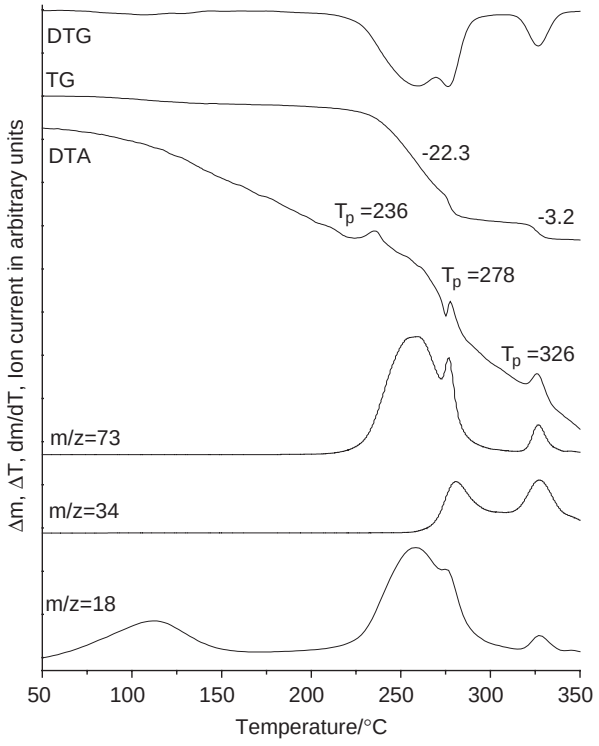

Fig. 7. DTA, TG, DTG and MS trend scan curves of $[Ni(dien)_2]Sb_4S_7 \cdot H_2O$ (**I**) (simultaneous measurement; dynamic helium atmosphere; weight: 29.3 mg; flow rate: 75 mL min^{-1}; $m/z = 18$: water/dien; $m/z = 34$: H_2S $m/z = 73$: dien; Al_2O_3 crucible; given are the mass changes (%) and the peak temperatures T_p in °C).

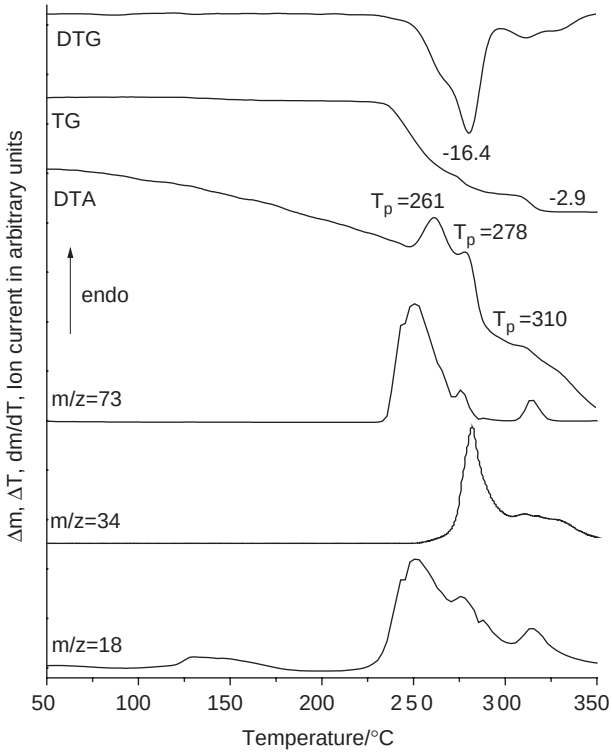

Fig. 8. DTA, TG, DTG and MS trend scan curves of $[Ni(dien)_2]_3Sb_{12}S_{21} \cdot H_2O$ (**II**) (simultaneous measurement; dynamic helium atmosphere; weight: 31.7 mg; flow rate: 75 mL min^{-1}; $m/z = 18$: water/dien; $m/z = 34$: H_2S $m/z = 73$: dien; Al_2O_3 crucible; given are the mass changes (%) and the peak temperatures T_p in °C).

X-ray powder pattern and additional reflections of an unknown phase were also observed. Elemental analysis reveals that the C, H, and N content is reduced to 2.3%, 0.4%, and 1.5%.

For $[Ni(dien)_2]_3Sb_{12}S_{21} \cdot H_2O$ a similar thermal behavior is found. Heating the sample a smooth decrease in the TG curve is observed between 60° and 180°C which corresponds to the emission of the water molecules ($m/z = 18$) (Fig. 8). The experimental mass loss of about 0.6% is in excellent agreement with that calculated ($-\Delta m_{theo}$1 $H_2O = 0.6\%$). On further heating at about 220°C a mass reduction of about 16.4% occurs which is accompanied by two endothermic events at 261°C and 278°C. From the DTG curve it is obvious that at least two different steps are involved which cannot be successfully resolved. However, in the first of these two reactions the organic ligands are removed ($m/z = 73$ and 18) whereas in the second step also H_2S ($m/z = 34$) is emitted. On further heating the mass decreases by another 2.9% being due to the emission of small amounts of dien and sulfur as H_2S. The total weight change of the three steps of 19.3% is smaller than expected for the complete removal of the ligands ($-\Delta m_{theo}$ 6 dien = 21.0%). Elemental analysis reveals that the black residue is contaminated by carbon, hydrogen, and nitrogen (C: 0.76%; H: 0.03%; N: 0.35%). In the X-ray powder pattern of the residue the compounds NiS, NiSbS and Sb_2S_3 could be identified and in the IR spectrum no C–H, C–N, C–C or N–H vibrations could be detected.

In further experiments decompositions were stopped at 256°C and 280°C. The residue isolated at 256°C was analyzed by X-ray powder diffraction and reflections of NiS, NiSbS and Sb_2S_3 occurred. The residue contains 5.1% C, 1.0% H and 3.6% N.

But again, no vibrations could be detected in the IR spectrum. If the reaction is stopped at 280°C only 2.0% C, 0.4% H and 1.2% N remain in the residue. In the X-ray powder pattern NiS, NiS_2, NiSbS, Sb_2S_3 were identified and weak reflections of an unknown phase. Interestingly, the decomposition products of $[Ni(dien)_2]Sb_4S_7 \cdot H_2O$ at $T = 274$°C and $[Ni(dien)_2]_3Sb_{12}S_{21} \cdot H_2O$ at 280°C are very similar.

3.4. Optical properties

The bonding properties of a lone pair atom are best detected from changes of the bond angles, whereas interatomic bond lengths are only slightly affected [35], and the local environment of the Sb(III) atoms exhibits no significant alterations of the Sb–S distances. Raman spectroscopy is a powerful tool for the detection of

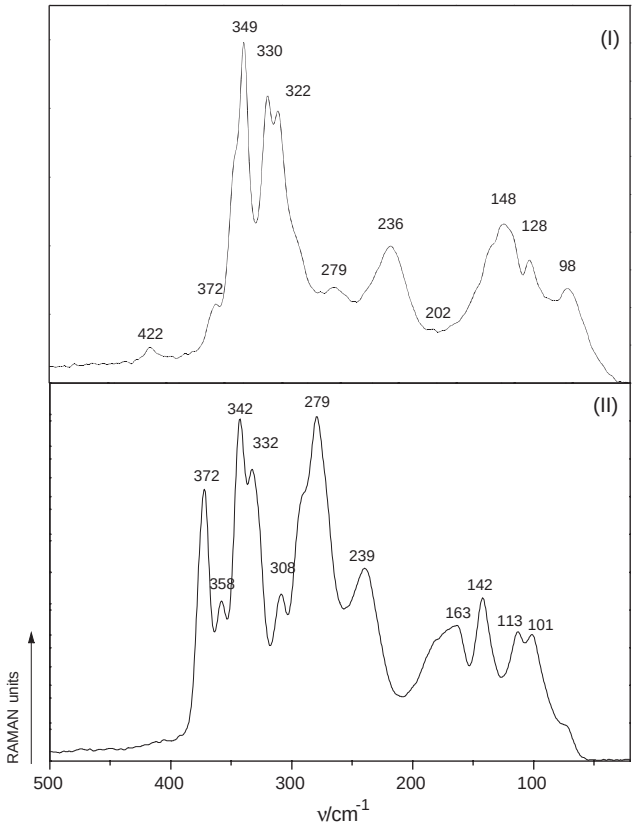

Fig. 9. Raman spectra of $[Ni(dien)_2]Sb_4S_7 \cdot H_2O$ (**I**) and $[Ni(dien)_2]_3Sb_{12}S_{21} \cdot H_2O$ (**II**).

differing bonding properties. The Raman spectra are shown in Fig. 9.

In **I** two SbS_3 units (Sb(1), Sb(2)) and two SbS_4 moieties with different Sb–S bond lengths and S–Sb–S angle are present. Strong modes are observed at 349, 330 and 322 cm^{-1} dominating the spectrum of $[Ni(dien)_2]Sb_4S_7 \cdot H_2O$. One resolved shoulder is found at 372 cm^{-1} and the resonance at 322 cm^{-1} has also a shoulder. The SbS_3 units with stronger bonding interactions, i.e. with the lower coordination number, give rise to the modes at higher energies [35].

The number of Sb_xS_y moieties in **II** as well as their environments are different than in **I**, and consequently the region of the Sb–S resonances in the Raman spectrum is quite different (Fig. 9). Strong modes are observed at 372, 342, 332, and 279 cm^{-1}. Between the bands at 372 and 342 cm^{-1} a less intense signal is located at 358 cm^{-1} and another weak band occurs at 332 cm^{-1}. A definite assignment of the resonances to the different SbS_x units cannot be given. But Sb(III) atoms with the higher coordination numbers show resonances at lower wave numbers.

Hence, the bands occurring in the region between 370 and 330 cm^{-1} are caused by SbS_x moieties with the lower number of Sb-S interactions. The assignment of the Sb-S modes are in accordance with the results reported by Pfitzner for Cu_3SbS_3 and $(CuI)_2Cu_3SbS_3$ [29]. In the former compound two maxima were observed at 321 and 290 cm^{-1} reflecting the weaker bonding interaction due to the $3+5$ environment. In the latter compound the $[SbS_3^{3-}]$ anion have no next-nearest S atoms yielding Raman bands at 362 and 339 cm^{-1}. For $MnSb_2S_4$ with one Sb(III) atom in a sixfold and the other Sb(III) atom in a sevenfold environment of S atoms Raman bands occur at even lower frequencies and are located between about 280 and 310 cm^{-1} [35].

In summary, two new thioantimonates(III) were synthesized under solvothermal conditions: the layered compound $[Ni(dien)_2]Sb_4S_7 \cdot H_2O$ (**I**) showing a different interconnection of the SbS_3 and SbS_4 primary units compared with the thioantimonates that also contain the $^2_\infty[Sb_4S_7^{2-}]$ anion. In **I** the condensation of the primary building units yields Sb_2S_2, Sb_4S_4, and Sb_8S_8 heterorings which may be viewed as secondary building blocks. The $^3_\infty[Sb_{12}S_{21}^{6-}]$ anion in compound **II** is composed of four SbS_3 pyramids and two SbS_4 units. The condensation of the different primary units yields Sb_2S_2, Sb_3S_3, Sb_4S_4, and Sb_8S_8 rings and the largest heteroring observed so far with the composition $Sb_{32}S_{32}$. The structure directing effect of the cations is obvious. In both compounds they are located above and below the pores formed by the larger Sb_xS_x heterorings ($x = 8$ in **I**, $x = 8$ and 32 in **II**). In **II** one cation resides in the plane of the large $Sb_{32}S_{32}$ ring. The pores in **II** are oriented parallel to the [110] direction and large tunnels run along [101]. From a synthetic point of view the observation that transition metal complexes act as structure directors opens new strategies for the successful syntheses of new thioantimonate compounds with new and unprecedented network architectures.

References

[1] H.A. Graf, H. Schäfer, Z. Naturforsch. B 27 (1972) 735.
[2] B. Eisenmann, H. Schäfer, Z. Naturforsch. B 34 (1979) 383.
[3] W.S. Sheldrick, H.-J. Häusler, Z. Anorg. Allg. Chem. 557 (1988) 105.
[4] G. Dittmar, H. Schäfer, Z. Anorg. Allg. Chem. 441 (1978) 93.
[5] G. Dittmar, H. Schäfer, Z. Anorg. Allg. Chem. 441 (1978) 98.
[6] G. Cordier, H. Schäfer, C. Schwidetzky, Z. Naturforsch. B 39 (1984) 131.
[7] G. Dittmar, H. Schäfer, Z. Anorg. Allg. Chem. 437 (1977) 183.
[8] J.B. Parise, Y. Ko, Chem. Mater. 4 (1992) 1446.
[9] M. Schur, W. Bensch, Eur. J. Solid State Inorg. Chem. t34 (1997) 457.
[10] W. Bensch, M. Schur, Z. Naturforsch. B 52 (1997) 405.
[11] H.-O. Stephan, M.G. Kanatzidis, Inorg. Chem. 36 (1997) 6050.
[12] X. Wang, F. Liebau, Acta Crystallogr. B 52 (1996) 7.
[13] F. Liebau, Structural Chemistry of Silicates, Springer, Berlin, 1985, p. 24ff.
[14] R. Stähler, C. Näther, W. Bensch, Acta Crystallogr. C 57 (2001) 26.

[15] R.C. Hynes, C.J. Willis, J.J. Vittal, Acta Crystallogr. C 52 (1996) 1879.
[16] G.M. Sheldrick, SHELXS-97, Program for structure solution, Universität of Göttingen, Germany, 1997.
[17] G.M. Sheldrick, SHELXL-97, Program for structure refinement, Universität of Göttingen, Germany, 1997.
[18] X-Shape, Program for numerical absorption correction, Version 1.03, Stoe & Cie, Darmstadt, Germany, 1998.
[19] W. Bensch, C. Näther, R. Stähler, Chem. Commun. 477 (2001).
[20] G.H. Searle, S.F. Lincoln, F.R. Keene, S.G. Teague, D.G. Rowe, Aust. J. Chem. 30 (1977) 1221.
[21] F.G. Mann, J. Chem. Soc. 466 (1934).
[22] F.R. Keene, G.H. Searle, Inorg. Chem. 11 (1972) 148.
[23] Y. Yoshikawa, K. Yamasaki, Bull. Chem. Soc. Jpn. 45 (1972) 179.
[24] G.H. Searle, D.A. House, Aust. J. Chem. 40 (1987) 361.
[25] A.K. Mukherjee, S. Koner, A. Ghosh, N.R. Chaudhuri, M. Mukherjee, A.J. Welch, J. Chem. Soc. Dalton Trans. 2367 (1994).
[26] F.S. Stephens, J. Chem. Soc. 883 (1969).
[27] K. Harada, Bull. Chem. Soc. Jpn. 66 (1993) 2889.
[28] R. Stähler, W. Bensch, J. Chem. Soc. Dalton Trans. 2518 (2001).
[29] A. Pfitzner, Chem. Eur. J. 3 (1997) 2032.
[30] X. Wang, F. Liebau, J. Solid State Chem. 111 (1994) 385.
[31] G.L. Schimek, J.W. Kolis, Inorg. Chem. 36 (1997) 1689.
[32] R. Stähler, W. Bensch, J. Chem. Soc. Dalton Trans. 2518 (2001).
[33] R. Stähler, C. Näther, W. Bensch, Eur. J. Inorg. Chem. 1835 (2001).
[34] A. Bondi, J. Phys. Chem. 68 (1964) 441.
[35] A. Pfitzner, D. Kurowski, Z. Kristallogr. 215 (2000) 373.